Spin dependence of $pp \rightarrow np\pi^+$ from 492 to 796 MeV

R. L. Shypit,* D. V. Bugg, and A. H. Sanjari
Queen Mary College, London E1 4NS, United Kingdom

D. M. Lee, M. W. McNaughton, and R. R. Silbar
Los Alamos National Laboratory, Los Alamos, New Mexico 87545

C. L. Hollas,† K. H. McNaughton, and P. Riley
University of Texas, Austin, Texas 78712

C. A. Davis
University of Manitoba, Winnipeg, Canada R3T 2N2
(Received 18 April 1989)

Spin correlation parameters A_{LL}, A_{SL}, A_{NL}, A_{NO}, A_{SO}, A_{LO}, and A_{OL} have been measured for $pp \rightarrow np\pi^+$ at 492, 576, 643, 729, and 796 MeV over a large part of phase space, using a longitudinally polarized target and a polarized beam. Results rule out broad dibaryons in this mass range in NN $^3P_2$ and $^3F_3$; in $^1D_2$ some phase variation is observed, resembling that expected of a strong inelastic threshold.

I. INTRODUCTION

Dibaryon resonances, if they exist, are highly inelastic.[1,2] Branching ratios to NN and πd are $<15\%$, and up to 800 MeV the remaining channel width can lie only in $NN\pi$ (which is dominatly $N\Delta$). The clearest signature of a dibaryon would therefore be a large and rapid phase variation with laboratory energy in a partial-wave amplitude for $NN \rightarrow N\Delta$. In the experiment reported here we have measured seven spin observables for the $pp \rightarrow np\pi^+$ reaction, six of which are sensitive to relative phases between partial-wave amplitudes. Our objective was to demonstrate whether or not dibaryons exist in this energy range. Results and an amplitude analysis have already been presented briefly by Shypit *et al.*[3] The present paper gives full experimental detail.

The notation used here for spin-dependent observables is as follows. As illustrated in Fig. 1, **L** is longitudinal, parallel to the beam momentum $\mathbf{p}_b$, **N** is normal to the production plane (which is defined here by the beam and the neutron direction $\mathbf{p}_n$, i.e., **N** is in the direction of $\mathbf{p}_b \times \mathbf{p}_n$), and **S** is sideways, in the direction of $\mathbf{N} \times \mathbf{p}_b$. For the asymmetry $A_{\alpha\beta}$, the first suffix refers to the beam and the second to the target.

The quantity σA_{NO} depends on the imaginary part of a product of amplitudes; an explicit expression is given in Sec. IV. In practice, the main terms are due to interference between the dominant $NN(^1D_2) \rightarrow N\Delta(^5S_2)$ amplitude and those originating from $^3P_1$, $^3P_2$, and $^3F_3$. These interferences depend on the three angles defining the final $NN\pi$ kinematic configuration in a way which is different and characteristic for every triplet amplitude. The quantity σA_{SL} is closely related and contains the real parts of precisely the same combination of amplitudes, though in addition it contains some terms given by moduli squared of partial-wave amplitudes. Thus, whatever the phases, measurement of both A_{NO} and A_{SL} guarantees precise phase information and determination of magnitudes as well.

Likewise, σA_{SO} and σA_{NL} depend on real and imaginary parts of another product of amplitudes [see Eqs. (4.5) and (4.6)]. The quantities σA_{LO} and σA_{OL} also depend on interferences, notably $^1D_2$ with $^3P_0$ and $^3P_2$. Thus, in total, six phase-sensitive observables have been measured. The observables A_{NL}, A_{SO}, A_{LO}, and A_{OL} are allowed by parity conservation to be nonzero when the final-state $p\pi^+$ is not coplanar with the production plane defined by the beam and the neutron.

The seventh quantity σA_{LL} depends on moduli squared of amplitudes, but with opposite signs (and different angular dependence) for singlet and triplet initial state with $J \geq L$. For example, singlet states or $^3P_0$ alone give $A_{LL} = -1$, while $^3F_3$ and $^3P_1$ states alone give $A_{LL} = +1$. Measurement of A_{LL} is crucial in fixing relative magnitudes of the large $^1D_2$, $^3F_3$, and $^3P_2$ amplitudes. In an earlier experiment at TRIUMF, Waltham *et al.*[4] found that A_{LL} depends strongly on the πN mass M, going from positive values near the πN threshold to large negative values in the Δ region. We confirm this result with greatly increased precision. This reveals a strong amplitude due to $NN(^3P_1) \rightarrow NS(^3S_1)$, where S stands for a πN S wave; this S wave amplitude is roughly independent of πN mass, and dominates over the Δ near the πN threshold. Interference between this wave and $NN \rightarrow N\Delta$ amplitudes provides further valuable phase information.

The history of dibaryons and the current situation are reviewed by Roos *et al.*[1] in the Particle Data Tables and by Locher *et al.*[2] The original stimulus came from the discovery by Auer *et al.*[5] of peaks and dips in $\Delta\sigma_L$. Hidaka *et al.*[6] and Hoshizaki[7] suggested the existence of $^3F_3$ and $^1D_2$ resonances, although Arndt[8] had suggested

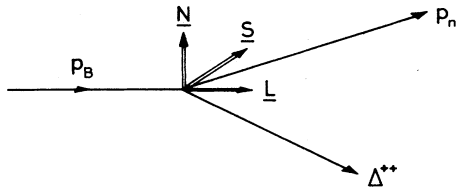

FIG. 1. Definition of **N**, **S**, and **L** vectors.

the possibility of the latter as early as 1968. Half-loops are seen in the Argand diagrams for $^1D_2$, $^3F_3$, and $^3P_2$. However, inelastic thresholds are difficult to distinguish from resonances; they give rise, via analyticity, to cusps, which, on the lower side of the threshold are very similar to the approach to a resonance. It is possible to explain present elastic data without resonances, as Kloet and Silbar,[9] Kloet, Tjon, and Silbar,[10] Niskanen,[11] VerWest,[12] and Furuichi *et al.*[13] argue. On the other hand, Edwards,[14] Bhandari *et al.*,[15] and recently Arndt *et al.*[16] conclude that there are poles in the elastic scattering amplitude at around 600-MeV beam energy. Kloet and Tjon[17] have presented a model where there is a pole close to the $N\Delta$ branch point, originating from left-hand singularities in the unphysical sheet (i.e., a resonance driven by the inelastic threshold).

One expects similarities between $pp \to d\pi^+$ and $pp \to np\pi^+$. However, the extra kinematic freedom in the latter is important in searching for dibaryons. The partial-wave amplitude for $pp \to n\Delta^+$ via π [one pion exchange (OPE)] exchange is given in the Born approximation by

$$f\alpha\frac{a(s)\Gamma(M)}{M_\Delta - M - i\Gamma(M)} . \tag{1.1}$$

Here s is the usual Lorentz invariant and M the πN mass. Initial- and final-state interactions modify $a(s)$ and a dibaryon resonance would introduce a pole into it. In $pp \to np\pi^+$, one can investigate separately dependence on s and M. In $pp \to d\pi^+$, this is not possible, since binding of the nucleons into the deuteron relates s and M. Amplitude analyses of $pp \to d\pi^+$ exist up to 800 MeV.[18,19] One sees a phase variation in $^1D_2$, $^3F_3$, $^3P_2$, and $^3P_1$ amplitudes which may be attributed to the denominator of Eq. (1). Several authors[20–22] however, ignore the Δ propagator and interpret the observed phase variation as a signature of a dibaryon resonance.

The present experiment grew out of an earlier measurement at TRIUMF by Waltham *et al.*, who measured A_{NO}, A_{ON}, A_{NN}, A_{LL}, A_{SS}, and A_{SL} at 425, 465, and 510 MeV with a geometry covering as much as possible of the aperture of a conventional polarized target. There, the energy was too restricted to draw definite conclusions about dibaryons.

At the Los Alamos Meson Physics Facility (LAMPF), pioneering efforts have been made to study the $np\pi^+$ channel by several groups. Cverna *et al.*[23] have used an unpolarized beam and target to measure $\pi^\pm$ spectra and angular distributions at 800 MeV. Hancock *et al.*[24] have measured $d\sigma/d\Omega$ and A_{NO} at 800 MeV over a range of geometries. Bhatia *et al.*[25] have measured A_{NN} and A_{LL} at 650 and 800 MeV over a range of geometries. Glass *et al.*[26] have measured K_{NN} and K_{LL} in $pp \to nX$ at 0° at 800 MeV. Hollas *et al.*[27] have measured Wolfenstein parameters at 800 MeV for proton angles 5°–10° and pion angles 80°–130°. There have been further measurements[28–30] of $pp \to pp\pi^0$ and some[31] which sum proton spectra over $pp\pi^0$ and $np\pi^+$; Bonner *et al.*[32] have measured cross sections for $np \to nX$.

At the Argonne ZGS, Wicklund *et al.*[33] have made high statistics measurements of A_{NO}, A_{LO}, and A_{SO} for $pp \to np\pi^+$ at 569, 806, 1012, and 1253 MeV. We shall demonstrate that our results agree closely with these results at 569 and 806 MeV.

The plan for this paper is as follows. Section II describes experimental details and Sec. III the data analysis. Section IV illustrates the features of the data. An amplitude analysis of data from the present experiment was reported by Shypit *et al.*[3] We shall not repeat that analysis here, but will point out the features of the data which lead to specific physics results. A more elaborate analysis, including all current $pp \to pp\pi^+$ and $pp\pi^0$ data, is in progress and will be reported separately.

II. THE EXPERIMENT

The experiment was done at LAMPF, using a longitudinally polarized propanediol target and a beam with polarization oriented successively in **N**, **S**, and **L** directions. The experimental setup is sketched in Fig. 2. All three final-state particles were detected in coincidence. The proton and π^+ were tracked in MWPC (multiwire proportional chambers) or drift chambers, covering as much as possible of the magnet aperture, and neutrons were detected in a position sensitive scintillator array 4.5 to 4.9 m from the target.

The Helmholz coils of the polarized target had a conical aperture of 48° half-angle upstream and downstream, and there was a further aperture of ±10.5° at 90°. Multiwire chambers were used downstream because of the high rates there; drift chambers (*C*, *D*, and *E* in Fig. 2) were used elsewhere. Each multiwire chamber consisted of a pair of planes, one horizontal and one vertical. The chamber closest to the target was 65 cm away and had an

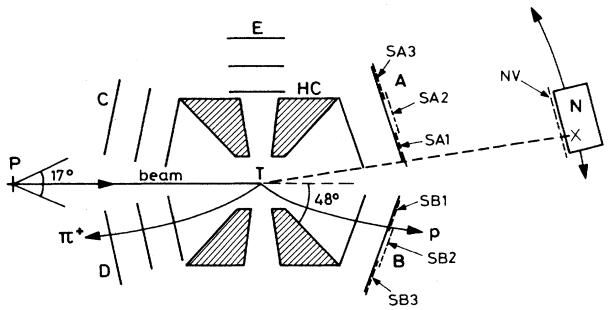

FIG. 2. A schematic plan view from above of the experimental layout. *A* and *B* are MWPC arms with trigger scintillators *SA*; *C*, *D*, and *E* are drift chamber arms. *HC* is the superconducting Helmholz coil of the polarized target *T*. *N* is the neutron detector, which moves through 25° on a radius arm. *NV* is the neutron veto. *P* is a polarimeter monitoring beam intensity, polarization, and spin orientation.

aperture of 38.4 cm horizontally $\times 51.2$ cm vertically with 2 mm wire spacing; the rear chamber was 25 cm further back and was 62.6 cm wide $\times 81.8$ cm high with 3 mm wire spacing. Their angular coverage was from 7.9° to 41° horizontally. Drift chambers also contained horizontal and vertical planes; three chambers were used in each arm with a spacing of 18 cm. Their active areas were 58.4 cm square.

Trigger scintillators were placed immediately behind the chambers. The five detector arms are named A,B,C,D,E as shown in Fig. 2. Triggers for $np\pi^+$ events were taken from combinations $A\cdot B$, $B\cdot B$, $B\cdot C$, $B\cdot D$, and $B\cdot E$. Other combinations gave no perceptible rate. Scintillators behind A and B arms were divided into three vertical strips and the $SA3\cdot SB3$ coincidence detected pp elastic events near 90° cm. Figure 3 displays a coplanarity distribution of events triggered by this coincidence; coplanarity is the dimensionless cross product of unit vectors in the directions of the beam and the two final protons. There is a clear hydrogen signal. This coincidence proved to be a valuable monitor of the centering of the beam on the target.

The neutron detector, sketched in Fig. 4, consisted of two layers, each 15 cm thick, of seven horizontal bars of scintillator, each 15 cm high by 105 cm long. Each scintillator was viewed from the two ends by photomultipliers; horizontal coordinates were deduced with ± 3.5 cm accuracy from relative timing of the pulses from the two photomultipliers. Constant fraction discriminators were used with thresholds set to 15 MeV. From previous experience in several experiments at TRIUMF the efficiency of the neutron detector is known to be about 25%. A scintillator shield in front vetoed charged particles with efficiency $\geq 99.9\%$. The time gate of the neutron counter was 80 ns wide to detect the full range of neutron energies. Time of flight τ was calculated off line with respect to (a) accelerator radio frequency (rf) and (b) trigger scintillators for p and π^+. The spacing between beam pulses was 5 ns. Thus (b) identified the pulse responsible for the event and (a) gave the most accurate determination of time of flight (rms $\delta\tau = 0.75$ ns). A small amount of data were taken with (a) missing, and the time-of-flight resolution then deteriorated to ± 1.3 ns.

At 800 MeV, nucleons from the $np\pi^+$ reaction lie within 52° of the beam and at lower energies are restricted to a smaller cone. Most of this range was sampled by positioning the neutron detector successively at three angles: 13°, 25°, and 37.5° at 800 MeV. This compares with 8°, 17°, 26°, and 35° in the earlier experiment at TRIUMF.

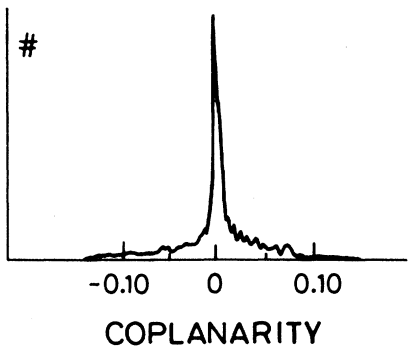

FIG. 3. Coplanarity distribution of events triggered by $SA3\cdot SB3$ at 796 MeV.

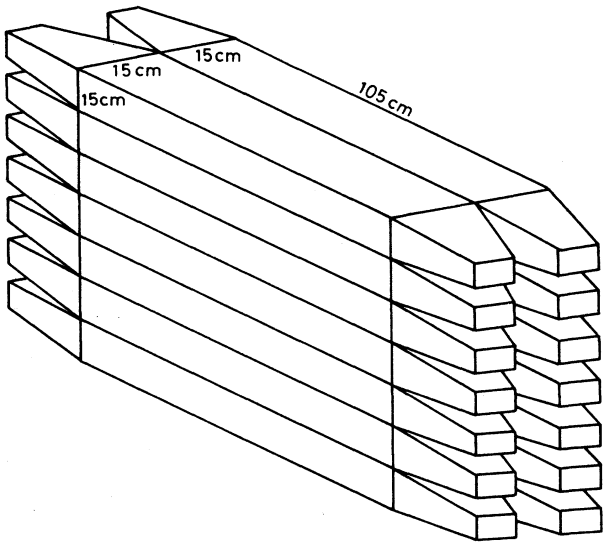

FIG. 4. The neutron array and its light guides.

Random triggers were monitored on line and kept below 10% by controlling beam intensity. Off line, random triggers contributed negligible background after kinetmatic reconstruction. Checks were made on the rate dependence of both the trigger and fully reconstructed events after background subtraction: for the maximum observed changes of 75% in rate, the ratio of accepted $np\pi^+$ events to beam counts showed variations less than statistics ($\pm 3\%$). These checks were independently verified in each of the relevant spin combinations. The ratio of beam intensities for + and − beam spin was monitored by an ionization chamber in the beam upstream of the target, with a precision of $\pm 1\%$. It was also checked by the polarimeter, though with lower accuracy. On some occasions, the focusing or centering of the beam on the target was imperfect. This was clearly identified during analysis by the ratio of N_{el}, the number of elastic events reconstructed from the $SA3\cdot SB3$ trigger to B, the beam recorded by the ionization chamber. This ratio monitors the proportion of incident beam hitting hydrogen in the target. When this ratio was unstable, data were discarded. However, on several occasions, the ratio fell (by a maximum of 15%) but remained stable within statistics (2%) over many runs. Rather than discarding such data, the beam count B was corrected by the observed ratio N_{el}/B averaged over at least one cycle of opposite beam polarizations, usually over many cycles. On such occasions, there was no significant change in the signal to background ratio for $np\pi^+$ events, so no correction was applied to the background subtraction there.

The beam was vertically polarized (**N**) at exit from the accelerator; its polarization was rotated to **N**, **S**, or **L** directions at the center of the polarized target by means

of a solenoid and bending magnets in the beamline. The polarimeter, with two horizontal and two vertical arms, checked the spin orientation. Whenever the polarization was perpendicular to **L**, the magnet of the polarized target rotated the polarization through a large angle, 45.56° at 492 MeV and 33.94° at 796 MeV; this rotation was calculated from the known $\int B_z dl = 1.04$ Tm from the exterior to the center of the magnet. The field was mapped accurately, and the integral was checked against the number of ampere turns of the magnet.

Beam polarization (typically 80%) was reversed every 2 min, and at this point the quench technique[34] was used to measure beam polarization for 5 s. This technique was statistically precise and is believed from past experience to have an absolute accuracy of ±1%. It was used for longitudinally polarized beam. The beam polarimeter had superior statistical accuracy, and was used for beam polarized in N and S directions.

The polarized target was 2 cm in diameter and 4 cm long. The material was propanediol, and polarization was typically 70% to 79%. Polarization was reversed several times for every beam energy and neutron counter setting. The polarization was monitored by standard NMR techniques, which are believed to have a reproducibility of ±1% and an absolute accuracy of ±4%. This estimate of target polarization was checked by measuring A_{LL} in pp elastic scattering at 90°; using values from Arndt's phase-shift analysis,[16] results agreed with the NMR measurement within the ±4% absolute accuracy. To avoid depolarizing the target by radiation damage, the target was changed at intervals, and, in between, the beam was steered over the area of the target in 2 mm steps vertically and horizontally. Background from heavy nuclei in the polarized target was measured at 492 and 796 MeV using a dummy target.

III. DATA PROCESSING

The first step was to calibrate the time-of-flight τ measured in the neutron detector. This was achieved using the prominent γ peak from $pp \to pp\pi^0$ and gave an rms value $\delta\tau = 0.75$ ns.

The input to the kinematics thus consisted of known directions for all three final-state particles at exit from the magnet, and the momentum of the neutron. Forward-going particles bent rather little in the magnetic field; treating their momenta as unknowns therefore gave a $2C$ fit. Backward-going pions were routinely reconstructed with bend angles up to 110° ($\equiv$70 MeV/c), and gave useful momentum information.

Kinematic fitting demanded a procedure fast enough to handle the 10^8 triggers, and therefore somewhat simpler than, say, that used for bubble chamber analysis. Directions of tracks at exit from the magnet were treated as exactly known. Only magnitudes of the momenta of the three outgoing particles were then fitted using an iterative procedure.

At first entry to the iterative process, momenta of charged particles were estimated from kinematic correlations and a detailed simulation of the setup. At every iteration these angles were corrected to the vertex using an accurate fast parametrization of bend angle in terms of momentum and direction; this parametrization was obtained by tracking a representative sample of particles

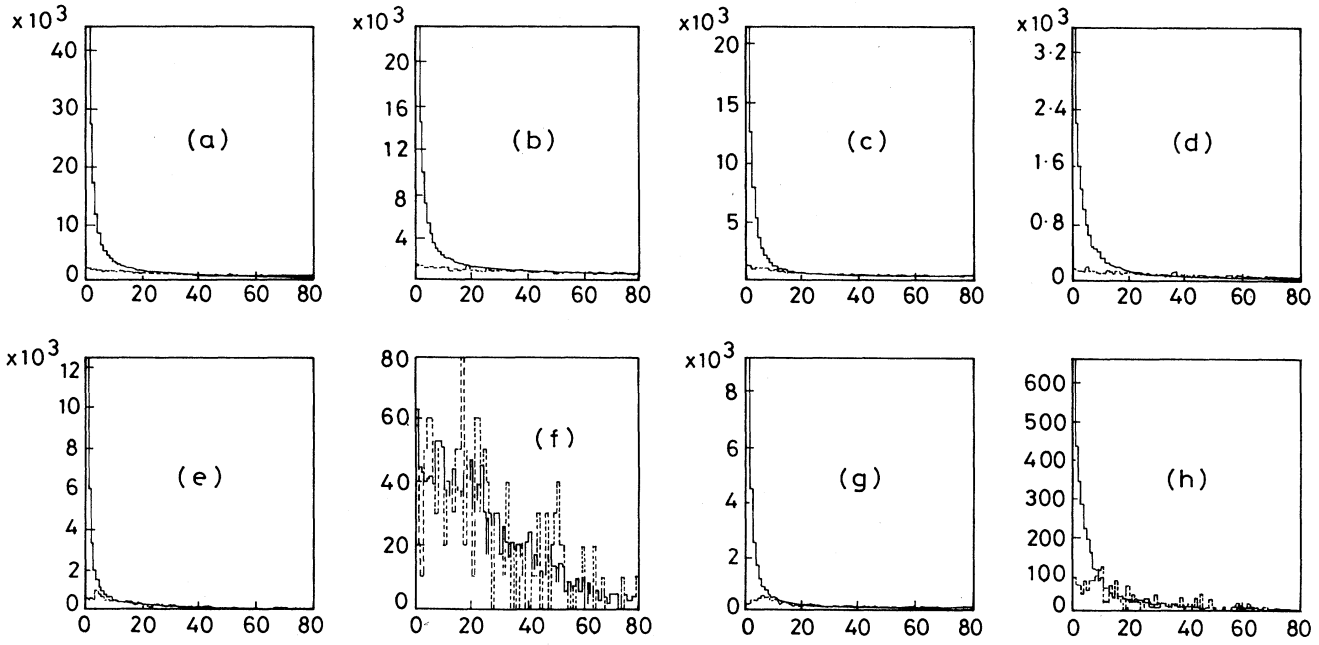

FIG. 5. χ^2 distributions, with background from the dummy target shown dashed, for $p\pi^+$ triggers (a) $A \cdot B$, (b) $B \cdot B$, (c) $B \cdot C$, (d) $B \cdot D$, and (e) $B \cdot E$ at 796 MeV, and (f) $B \cdot C$, (g) $A \cdot B$, (h) $B \cdot B$ at 492 MeV. The neutron counter was at 25° for (b) and (g) and at 13° for the rest.

numerically. The quantity

$$\chi^2 = \left[\frac{\Delta P_x}{\delta P_x}\right]^2 + \left[\frac{\Delta P_y}{\delta P_y}\right]^2 + \left[\frac{\Delta P_z}{\delta P_z}\right]^2 + \left[\frac{\Delta E}{\delta E}\right]^2 + \left[\frac{\tau_f - \tau_m}{\delta \tau}\right]^2 \tag{3.1}$$

was minimized iteratively. Here $\Delta P_{x,y,z}$ and ΔE are imbalances of momentum components and energy at the vertex and $\tau_{f,m}$ are fitted and measured times of flight of the neutron. The value $\delta E = 1$ MeV was chosen to demand energy conservation; $\delta P_{x,y,z}$ were set to 10, 15, 10 MeV/c for $A\cdot B$ and $B\cdot B$ combinations of trigger and 15, 20, and 15 MeV/c for the other combinations which involved pions in the C, D, and E arms. With these values, hydrogen events followed closely the χ^2 distribution for 2 degrees of freedom (except that the χ^2 signal was somewhat degraded for protons of the lowest momentum). The target was treated as a point source. Carbon events, where Fermi momenta are typically 120 MeV/c along each axis, gave a nearly flat distribution in χ^2 up to values > 100. The procedure converged typically in three iterations.

Figure 5 shows χ^2 distributions for $A\cdot B$, $B\cdot B$, $B\cdot C$, $B\cdot D$, and $B\cdot E$ triggers at 796 and 492 MeV; dashed lines are measured with the dummy target. There is a clear hydrogen signal. The $B\cdot B$ configuration with the neutron detector at 13° is suppressed by phase space, so we display results for the 25° neutron location. At 492 MeV, $B\cdot C$, $B\cdot D$, and $B\cdot E$ triggers give no significant signal, as anticipated from Monte Carlo simulations, because pion momenta are so low that the particles are trapped close to the beam.

No dummy target data were taken at 576, 643, and 729 MeV, so background shapes were interpolated between 492 and 796 MeV, and normalized to data with $\chi^2 > 30$. As expected, because of smearing by Fermi motion, the background varied more slowly with kinematic variables (e.g., $p\pi^+$ or np invariant mass) than for hydrogen events.

Hydrogen events were selected by a cut $\chi^2 < 8$. With this cut, there remained 381 K events summed over spin configurations at 796 MeV, 235 K at 733 MeV, 262 K at 643 MeV and 108 K at 492 MeV. A clear signal was observed in C, D, and E arms down to 643 MeV and in the E arm at 576 MeV. At 492 MeV, the signal was confined to $A\cdot B$ and $B\cdot B$ triggers for neutron detector settings of 13° and 25°, as Monte Carlo simulations predicted. The limited coverage of phase space at 492 MeV leads to some ambiguities in the eventual amplitude analysis.

Chamber efficiencies ϵ were obtained, run by run for each arm, from the ratio of triggers to reconstructed hits in the chambers. There was no evidence for variation of efficiencies over the area of the chambers.

The determination of asymmetries proceeded in two stages. First, raw asymmetries A_B, A_T, and A_{BT}, corresponding to beam, target, or both being polarized, were calculated from the following equations:

$$\begin{aligned}
I^{++} &= \eta N^{++}(1 + A_B P_B^{++} + A_T P_T^{++} \\
&\quad + A_{BT} P_B^{++} P_T^{++})(1 + B^{++})\epsilon^{++}, \\
I^{-+} &= \eta N^{-+}(1 - A_B P_B^{-+} + A_T P_T^{-+} \\
&\quad - A_{BT} P_B^{-+} P_T^{-+})(1 + B^{-+})\epsilon^{-+}, \\
I^{+-} &= \eta N^{+-}(1 + A_B P_B^{+-} - A_T P_T^{+-} \\
&\quad - A_{BT} P_B^{+-} P_T^{+-})(1 + B^{+-})\epsilon^{+-}, \\
I^{--} &= \eta N^{--}(1 - A_B P_B^{--} - A_T P_T^{--} \\
&\quad + A_{BT} P_B^{--} P_T^{--})(1 + B^{--})\epsilon^{--},
\end{aligned} \tag{3.2}$$

where I and N are event and beam rates, respectively, P_B and P_T are magnitudes of beam and target polarizations, and η is an overall proportionality constant which cancels out of asymmetries; the first and second superscripts indicate polarities of beam and target polarizations. The B's are background signal ratios; the background is independent of target polarization, since heavy nuclei are unpolarized. These equations are solved for every one of the bins described in Sec. III A; however, to eliminate noise in the background subtraction, the B's are determined only for each setting of the neutron counter and each trigger combination.

If beam polarizations were perfectly aligned normal to the nX^{++} plane, or sideways in the plane or longitudinally, this would complete the determination of asymmetries. However, in practice, one has to allow for small misalignments of two sorts. First, misalignments of beam steering gave rise to small components of beam polarization in unwanted directions; these were determined by the polarimeter. Secondly, individual events lie in planes making an angle ψ to the horizontal and one has to resolve beam polarization onto this plane; the magnetic field deflected slow pions quite significantly, and rotated the effective acceptance out of the horizontal plane. Suppose the beam polarization has components P_B^x horizontally to the left, P_B^y vertically upwards, and P_B^z longitudinally. Then averaging over events and taking the asymmetry A_{BT} as an example,

$$\begin{aligned}
P_B A_{BT} &= A_{SL}(\langle \cos\psi \rangle P_B^x + \langle \sin\psi \rangle P_B^y) \\
&\quad + A_{NL}(-\langle \sin\psi \rangle P_B^x) + \langle \cos\psi \rangle P_B^y) \\
&\quad + A_{LL} P_B^z .
\end{aligned} \tag{3.3}$$

When the beam is polarized nearly horizontally, P_B^x dominates, and $A_{BT} \simeq A_{SL}$; in this case, terms in (3.3) after the first are minor perturbations. Likewise, when the beam is nearly vertically polarized, the term $A_{NL}\langle \cos\psi \rangle P_B^y$ dominates. Nonetheless, the three equations with the form of (3.3) were solved simultaneously for the observables A_{SL}, A_{NL}, and A_{LL}. Equations similar in form to (3.3) apply to the raw asymmetries A_B and A_T.

A useful check on this procedure is that A_{OL} is determined three times, with the beam polarized horizontally, vertically, and longitudinally. Discrepancies between these three determinations are everywhere at the level of the statistical error. If one sums over geometries, the sta-

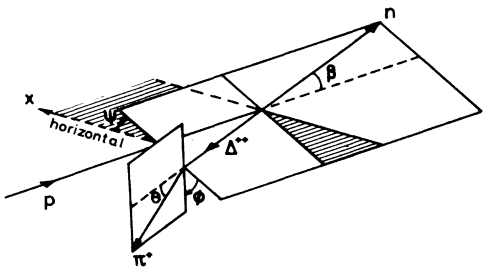

FIG. 6. Illustration of the angles β, θ, and ϕ.

tistical error on the mean A_{OL} is typically ± 0.015, so this is quite an accurate check.

A. Binning of data

The physics is dominated by $NN \rightarrow N\Delta$ and the amplitude for $pp \rightarrow n\Delta^{++}$ has an isospin Clebsch-Gordan coefficient three times that for $pp \rightarrow p\Delta^{+}$. Hence it is useful to use $M = p\pi^{+}$ mass as one kinematic variable. The remaining variables may be chosen as the angles β, ψ, θ, and Φ shown in Fig. 6; β is the center-of-mass (c.m.) angle of the neutron, and θ and Φ are polar angles of the π^{+} in the $(p\pi^{+})$ rest frame with $\Phi = 0$ when the π^{+} is in the $n\Delta^{++}$ production plane. By projecting beam polarization with respect to the production plane, we have defined $\psi = 0$. Another variable which will be useful in looking for the effect of NN final-state interactions is the np mass M_{NN}.

One gets a global impression of the coverage of phase space by projecting events into one-dimensional histograms against M, M_{NN}, $\cos\beta$, $\cos\theta$, and Φ, as well as momenta of n, p, and π^{+}, and neutron transverse momentum p_T^n. Results at 796 MeV are shown in Fig. 7 and are largely self-explanatory. The dips in the Φ histogram come from loss of pions moving vertically, and are rotated somewhat from 90° and 270° by the longitudinal field of the polarized target. The pion momentum spectrum shows a low momentum peak corresponding to events with the pion going into the backward arms C and D (see Fig. 2).

The histogram against NN mass shows a small peak at low mass due to final-state interactions. This is less pronounced than that observed in the earlier TRIUMF experiment for kinetmatic reasons. The smallest angle of the neutron counter was 13° at LAMPF and 8° at TRIUMF, and low NN mass requires a fast pion on the other side of the beam; the acceptance for such events is low. Careful checks show that this peak does not originate from protons in the A arm breaking through the veto of

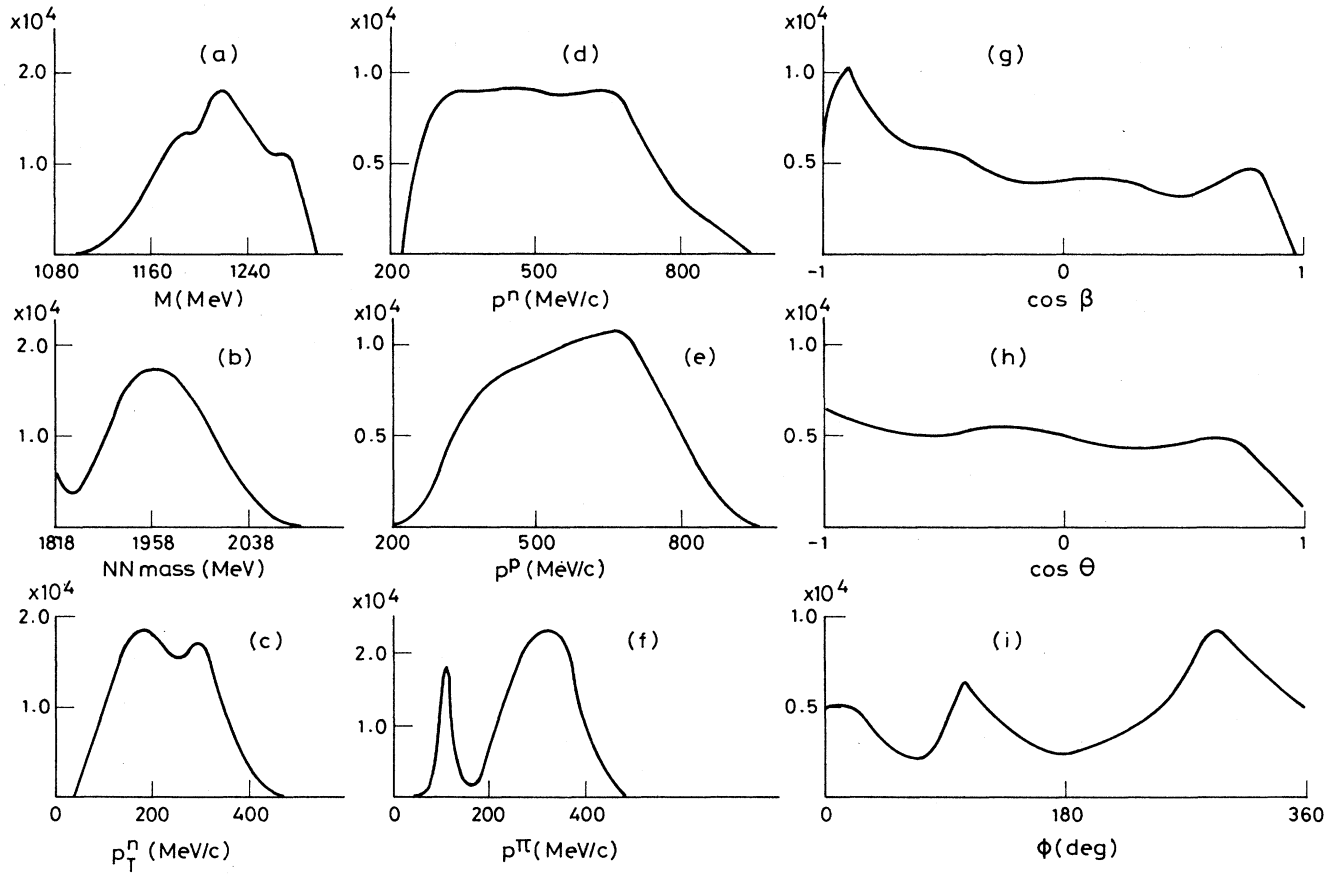

FIG. 7. One-dimensional projections of the number of events at 796 MeV onto (a) $M = p\pi^{+}$ mass, (b) NN mass, (c) neutron transverse momentum p_T^n, momenta of (d) n, (e) p, and (f) π^{+}, and (g) $\cos\beta$, (h) $\cos\theta$, and (i) ϕ.

the neutron counter. This final-state interaction peak is also visible at 729 and 643 MeV.

In order to extract the physics, events have been binned at each beam energy into $5\times5\times3\times4$ bins of M, $\cos\beta$, $\cos\theta$, and Φ, but data in overlapping bins from neutron counter positions of 13°, 25°, and 37° have been kept separate. The result is 163 bins with significant statistics at 492 MeV and 296 at 796 MeV. Of these, 69 have 1000 or more hydrogen events at 796 MeV. Tapes or listings (2000 lines) of these four-dimensional results are available on request.

In the amplitude analysis a detail is that partial-wave amplitudes are averaged over nine points in each bin: the center value of the bin population in each dimension and points ± half the distance to the nearest bin edge; each point is weighted by its calculated cross section. This has the effect of reducing the fitted χ^2 by 5% compared with using the central point only.

IV. FEATURES OF THE DATA

Let the amplitudes be $F_{\pm\pm}$ for beam and target spins $\pm\frac{1}{2}$ in the L direction. Since spins are not observed in the final state in this experiment, we suppress their indices and imply a summation over final spins. Then the unpolarized cross section is given by

$$4\sigma = \mathrm{Tr}(F^*F) = |F_{++}|^2+|F_{+-}|^2+|F_{-+}|^2+|F_{--}|^2 \tag{4.1}$$

and spin correlations by

$$4\sigma A_{\alpha\beta} = \mathrm{Tr}(F^*\sigma_\alpha\sigma_\beta F)\ . \tag{4.2}$$

Explicitly,

$$4\sigma A_{NO} = -2\,\mathrm{Im}(F^*_{++}F_{-+} - F^*_{+-}F_{--})\ , \tag{4.3}$$

$$4\sigma A_{SL} = 2\,\mathrm{Re}(F^*_{++}F_{-+} - F^*_{+-}F_{--})\ , \tag{4.4}$$

$$4\sigma A_{SO} = 2\,\mathrm{Re}(F^*_{++}F_{-+} + F^*_{+-}F_{--})\ , \tag{4.5}$$

$$4\sigma A_{NL} = 2\,\mathrm{Im}(F^*_{++}F_{-+} + F^*_{+-}F_{--})\ , \tag{4.6}$$

$$4\sigma A_{LO} = |F_{++}|^2+|F_{+-}|^2-|F_{-+}|^2-|F_{--}|^2\ , \tag{4.7}$$

$$4\sigma A_{OL} = |F_{++}|^2-|F_{+-}|^2+|F_{-+}|^2-|F_{--}|^2\ , \tag{4.8}$$

$$4\sigma A_{LL} = |F_{++}|^2-|F_{+-}|^2-|F_{-+}|^2+|F_{--}|^2\ . \tag{4.9}$$

Singlet initial states contribute to $(F_{+-}-F_{-+})$, $^3P_0$ to $(F_{+-}+F_{-+})$, triplet states with $L=J$ (e.g., $^3P_1$ and $^3F_3$) to $(F_{++}-F_{--})$, $^3P_2$ to $[F_{++}+F_{--}+2(F_{+-}+F_{-+})/\sqrt{3}]$ and $^3F_2$ to $[F_{++}+F_{--}-\sqrt{3}(F_{+-}+F_{-+})]$. From these expressions, one can read off from (4.3) to (4.9) the contributions of each partial wave to the observables.

Clearly A_{NO} and A_{NL} depend on interferences between partial waves. Observables A_{SL} and A_{SO} are closely related to A_{NO} and A_{NL}, but in addition to interferences, contain contributions from moduli squared of $^3P_2$ and $^3F_2$ and higher waves with initial $L=J\pm1$. Observables A_{LO} and A_{OL} involve only interferences, as we now show. Jacob and Wick[35] show from parity conservation that for any partial wave $F^*_{++}=\pm F_{--}$ and $F^*_{+-}=\pm F_{-+}$. Consequently, moduli squared of partial-wave amplitudes drop out of A_{LO} and A_{OL}.

At low energies, S-wave $N\Delta$ and NS final states dominate, and as the energy rises strong $N\Delta$ P-wave amplitudes come into play. From 492 to 643 MeV, the largest two amplitudes are $NN(^1D_2)\to N\Delta(^5S_2)$ and $NN(^3P_1)\to NS(^3S_1)$. Their interference dominates A_{NO}, A_{SL}, A_{SO}, and A_{NL}. At higher energies, further large interferences between the $^1D_2$ initial state and $^3P_1$, $^3P_2$, $^3F_2$, and $^3F_3$ $NN\to N\Delta$ amplitudes appear. The differences between A_{SO} and A_{SL} and between A_{NO} and A_{NL} separate $^3P_1$ and $^3F_3$ from $^3P_2$ and $^3F_2$. The dependence on $\cos\beta$ separates $^3P_1$ from $^3F_3$. This is true also, in principle, for $^3P_2$ and $^3F_2$, but in practice the latter is a small amplitude and can be lost in the uncertainties of $^3P_2$; we find a clean separation only at 796 MeV. This follows the pattern of experience[18] in analyzing $pp\to d\pi^+$, where the $^3F_2$ amplitude has proved the most difficult to determine of the low partial waves.

Observables A_{LO} and A_{OL} are valuable because they contain interferences between $^1D_2$ and $^3P_0$, absent from A_{NO}, A_{SO}, A_{NL}, and A_{SL}. However, only the real parts of interference terms are present; a measurement of A_{SN} and/or A_{NS} would determine the imaginary parts of the same interference terms. Measurements of A_{NN} and A_{SS} would also be useful.

From the data of the present experiment, it is hard to determine with any accuracy the $NN(^1S_0)\to N\Delta(^5D_0)$ amplitude, and likewise $^1D_2\to{}^3D_2$ and $^1D_2\to{}^5D_2$. All depend on initial spins in the same way as the dominant $^1D_2\to{}^5S_2$ amplitude. They are weak and distinguished only by angular dependence in the final state. The $^1G_4\to{}^5D_4$ amplitude rises to 25% of the $^1D_2\to{}^5S_2$ amplitude at 800 MeV, and amplitude analysis confirms that its strength is within 10% of OPE at this energy. Consequently, the amplitude analysis takes waves with final-state orbital angular momentum $L'=2$ from OPE; when further data are added to the analysis, it may be possible to determine these partial waves from experiment.

We refer to Shypit *et al.*[3] for fitted partial-wave amplitudes. The phase of each partial wave is expressed there in the form $[\delta_{NN}(s)+\delta_{N\Delta}(s)]$, where δ_{NN} is the NN elastic phase shift. Results for $\delta_{N\Delta}$, which are the essential indicators of the presence or absence of dibaryons, are displayed in Figs. 8 and 9. Ryskin and Strakovsky[36] have

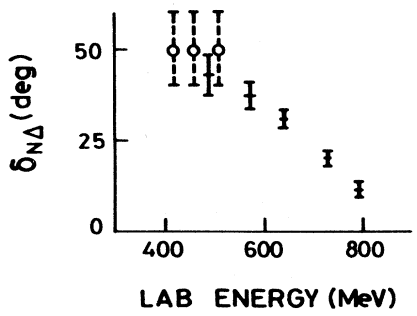

FIG. 8. The phase $\delta_{N\Delta}$ for $^1D_2\to{}^5S_2$; dashed values are from Ref. 4.

commented that there might be an overall phase ambiguity, common to all partial waves, and allowing resonant behavior in all the large partial waves. In our reply,[37] we have pointed out that the $NN(^1G_4)\rightarrow N\Delta(^5D_4)$ and $NN(^3H_5)\rightarrow N\Delta(^5F_5)$ amplitudes due to OPE are sufficiently strong at 643 MeV and above to act as a powerful interferometer, determining absolute phases and ruling out this possibility.

The form of the dependence of the data on θ, Φ, and β will be discussed next. In this energy range, only πN S and P waves are significant. The P waves give spin nonflip amplitudes varying as $\cos\theta$ and spin-flip amplitudes varying as $\sin\theta\exp(\pm i\Phi)$; S waves give only nonflip amplitudes independent of θ and Φ. It follows that the most general form for the dependence of the cross section on θ and Φ is[33]

$$d^4\sigma/dM\,d(\cos\beta)d(\cos\theta)d\phi=\rho_{11}(1+3\cos^2\theta)+\rho_{33}(3\sin^2\theta)-\sin\theta\cos\theta(\rho_{31}\cos\Phi+\rho'_{31}\sin\Phi)$$
$$-\sin^2\theta(\rho_{3-1}\cos2\Phi+\rho'_{3-1}\sin2\Phi)+\rho_{s1}\cos\theta+\sin\theta(\rho_{s-1}\cos\Phi+\rho'_{s-1}\sin\Phi)+\rho_s\ . \qquad (4.10)$$

Unpolarized cross sections and A_{NO}, A_{SL}, and A_{LL} contribute to unprimed density-matrix elements ρ, while A_{SO}, A_{LO}, A_{OL}, and A_{NL} contribute to ρ', i.e., to noncoplanar events. The ρ_{11}, ρ_{33}, ρ_{31}, ρ_{3-1}, ρ'_{31}, and ρ'_{3-1} arise from squares of πN P waves and from interference between $P_{1/2}$ and $P_{3/2}$; each term is a function of $\cos\beta$ depending on the L,J of initial NN states and L',S' of final NX states, where $X=\pi N$. The terms ρ_{s1}, ρ_{s-1}, and ρ'_{s-1} arise from interference between πN S and P waves, and ρ_s arises from S waves squared.

The amplitude analysis fits the full four-dimensional form of the data, of course. However, the main features may be appreciated from one-dimensional projections. Figures 10–12 show such projections of A_{LL}, A_{NO}, and A_{SL}. The full lines on the figures show representative fits from the amplitude analysis; note that they are not necessarily symmetric forward and backward, because the acceptance is asymmetric.

The asymmetry A_{LL} is quite revealing. It is easy to show from Eq. (4.9) that $A_{LL}=-1$ for a pure singlet state, while for a pure initial $^3P_1$ or $^3F_3$ state $A_{LL}=+1$. Figures 10(a) and 10(e) show that the $^1D_2\rightarrow{}^5S_2$ amplitude dominates at low beam energies for values of M approaching the Δ mass. But at the lowest M values, A_{LL} rises dramatically due to a strong $NN(^3P_1)\rightarrow NS(^3S_1)$ amplitude, leading to the πN S state. At 643, 729, and 796 MeV, A_{LL} rises at all angles, due to a rapid rise of $^3P_2\rightarrow{}^3P_2$, $^3P_2\rightarrow{}^5P_2$, and $^3F_3\rightarrow{}^5P_3$ $NN\rightarrow N\Delta$ amplitudes. The A_{LL} parameter is important in separating the strength of the $^1D_2$ amplitude from these others.

The asymmetry A_{NO} is large at 492 MeV and gets smaller at 796 MeV. This behavior was observed by Wicklund *et al.* Also A_{SL} shows some tendency to get larger at the higher energies. As discussed above, A_{NO} depends on the imaginary parts of interferences of $^1D_2\rightarrow{}^5S_2$ with $^3F_3$, $^3P_1$, and, to a lesser extent, $^3P_2$ amplitudes, while A_{SL} contains the real parts of the same in-

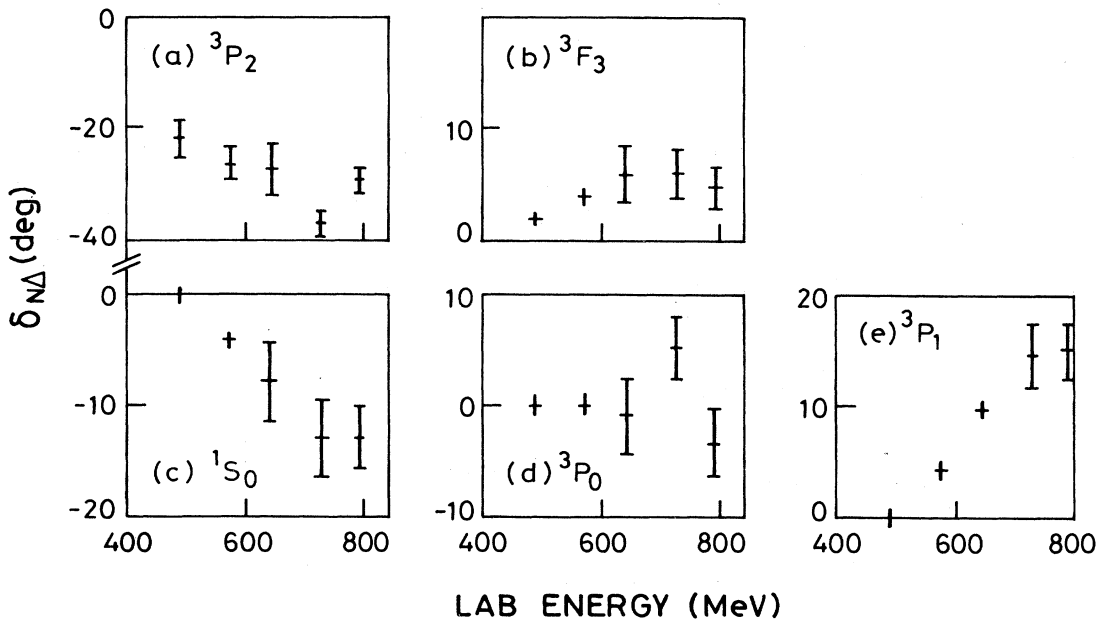

FIG. 9. Phases $\delta_{N\Delta}$ for (a) $^3P_2\rightarrow{}^3P_2$ and $^5P_2$, (b) $^3F_3\rightarrow{}^5P_3$, (c) $^1S_0\rightarrow{}^5D_0$, (d) $^3P_0\rightarrow{}^3P_0$, and (e) $^3P_1\rightarrow{}^3P_1$ and $^5P_1$.

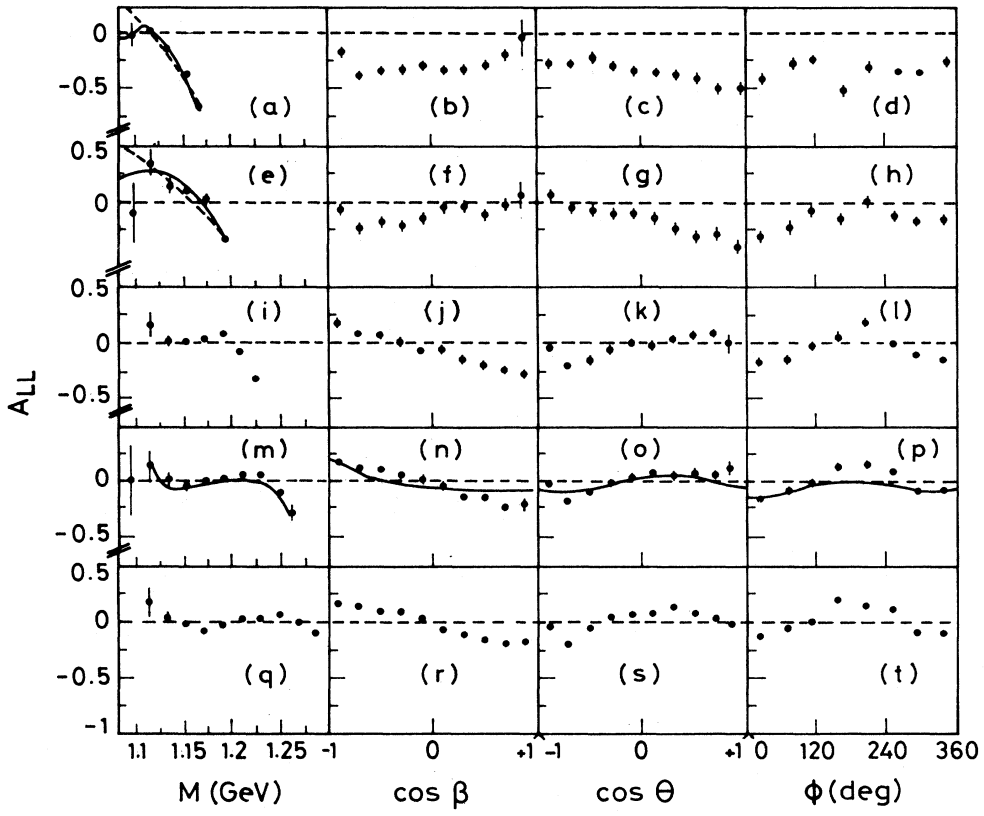

FIG. 10. One-dimensional projections of A_{LL} against M, $\cos\beta$, $\cos\theta$, and ϕ at (a)–(d) 492 MeV, (e)–(h) 576 MeV, (i)–(l) 643 MeV, (m)–(p) 729 MeV, and (q)–(t) 796 MeV. The full lines indicate fitted values summed over our acceptance. The dashed curves illustrate the effect of discarding the $\pi N S_{11}$ amplitude but keeping S_{31}.

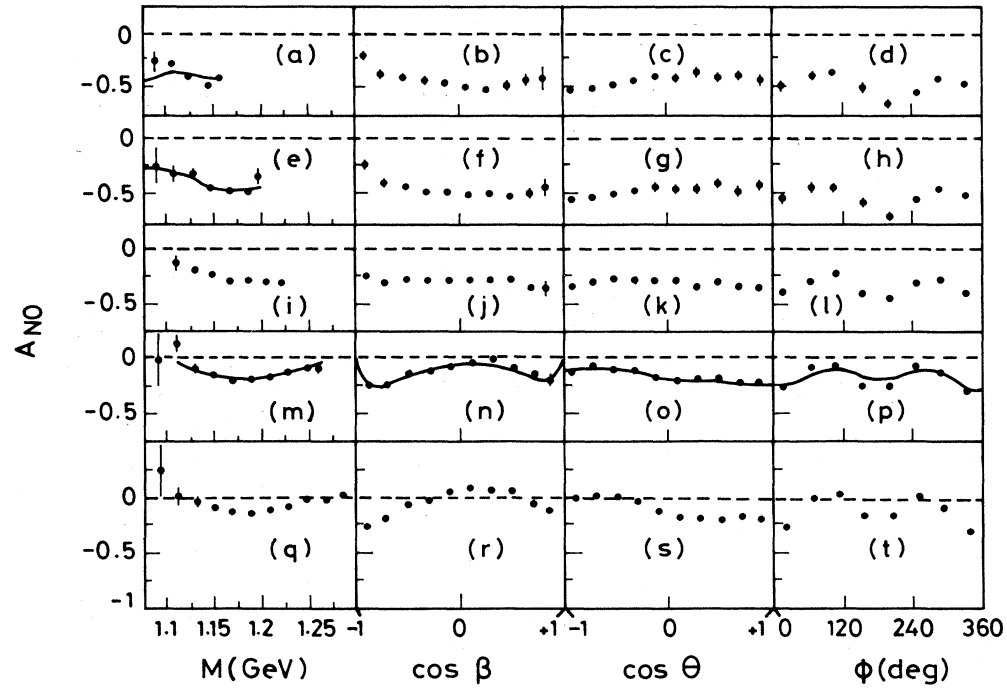

FIG. 11. As Fig. 10 for A_{NO}.

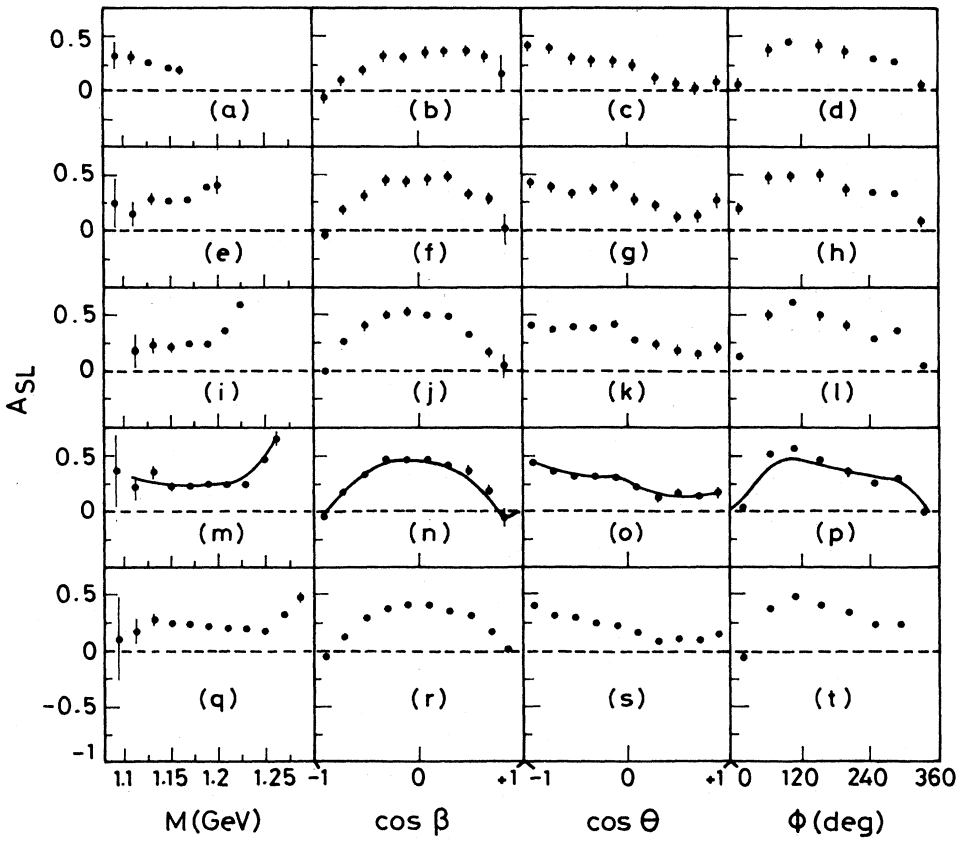

FIG. 12. As Fig. 10 for A_{SL}.

terference terms. The large values of A_{NO} at 492 MeV immediately require the $NN(^1D_2)\rightarrow N\Delta(^5S_2)$ and $NN(^3P_1)\rightarrow NS(^3S_1)$ amplitudes to be approximately orthogonal. Since the phase of the latter is about $-40°$, the phase of the former must be about $+50°$. The fit gives $\delta N\Delta(^5S_2)=44°$. The decrease in A_{NO} at the higher energies demands a variation of the phase of the $^1D_2\rightarrow{}^5S_2$ amplitude with respect to the other amplitudes. The amplitude analysis shows that it is the $^1D_2$ amplitude which is changing, and at 796 MeV, $\delta N\Delta(^5S_2)$ has fallen to 11°. This is an important result. We speculate in Sec. V that the behavior of $\delta_{N\Delta}(^5S_2)$ arises via analyticity from the step in $\mathrm{Im}f(N\Delta\rightarrow N\Delta)$ at threshold.

Observables A_{SO}, A_{LO}, A_{OL}, and A_{NL} appear only in terms depending on $\sin\Phi$. Figures 13–15 show averages of these observables (and A_{NO} for comparison) weighted by $\sin\theta\sin\Phi$, $\sin2\theta\sin\phi$, and $\sin^2\theta\sin2\Phi$. If the acceptance were uniform, these and similar projections would determine the density matrices ρ and ρ' as functions of $\cos\beta$, as was done in Ref. 33. Our acceptance is far from uniform, and Figs. 13–15 serve to give a rough picture of (a) the energy dependence and (b) which observables are large and which small. On the whole, variations with energy are rather small. Bearing in mind that these observables are phase sensitive, the small energy dependence leaves little scope for accommodating broad dibaryon resonances, unless they conspire in a quite remarkable way. Indeed, the amplitude analysis shows that the observed variations originate almost entirely from phase variations in the $^1D_2\rightarrow{}^5S_2$ amplitude, and the phases of most other amplitudes vary little. This is characteristic of the onset of an inelastic threshold.

Wicklund *et al.* determined density-matrix elements from their measurements of A_{SO}, A_{NO}, and A_{LO} at 806 MeV summed over the range $M=1180$ to 1280 MeV covering the Δ, and at 569 MeV summed over the range 1160 to 1200 MeV. Their results may be compared with ours in two ways. Figure 13 shows (crosses) predictions calculated from their published density-matrix elements averaged over our acceptance; the difference of a few MeV in beam energy between the two experiments is insignificant. The agreement is excellent. Secondly, we use their tables to evaluate A_{NO}, A_{SO}, and A_{LO} at the center of our bins, and form

$$\chi^2=\sum_i(\text{discrepancy})_i^2/(\text{error}_1^2+\text{error}_2^2)_i\ , \qquad (4.11)$$

where the errors refer to the two experiments. Results are given in Table I. There is good agreement.

The amplitude analysis also reveals good agreement with the A_{NO} data of Hancock *et al.*[24] in the regions of phase space where they overlap. The latter experiment checked normalization with errors of $\pm3\%$ by also measuring *pp* elastic scattering. The agreement of our re-

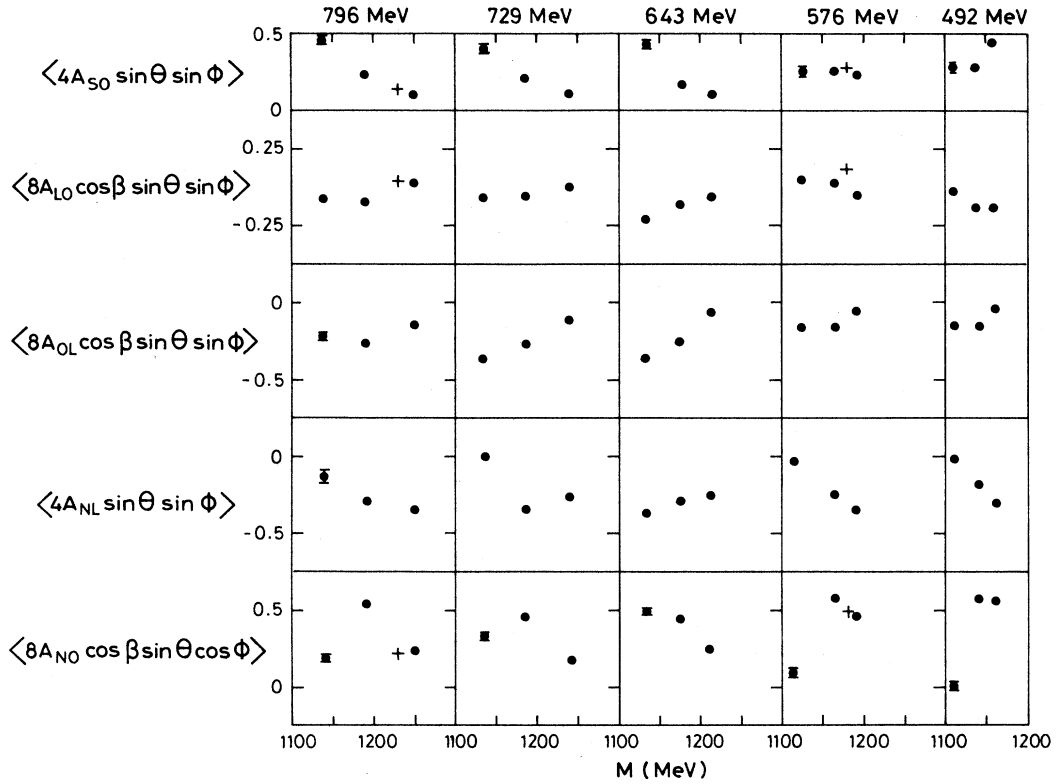

FIG. 13. Circles indicate averages over our acceptance $\langle 4A_{SO}\sin\theta\sin\Phi\rangle$, $\langle 8A_{LO}\cos\beta\sin\theta\sin\Phi\rangle$, $\langle 8A_{OL}\cos\beta\sin\theta\sin\Phi\rangle$, $\langle 4A_{LL}\sin\theta\sin\Phi\rangle$, and $\langle 8A_{NO}\cos\beta\sin\theta\cos\Phi\rangle$ plotted against $p\pi^+$ mass M; crosses indicate values of Wicklund *et al.* (Ref. 33) averaged over this acceptance.

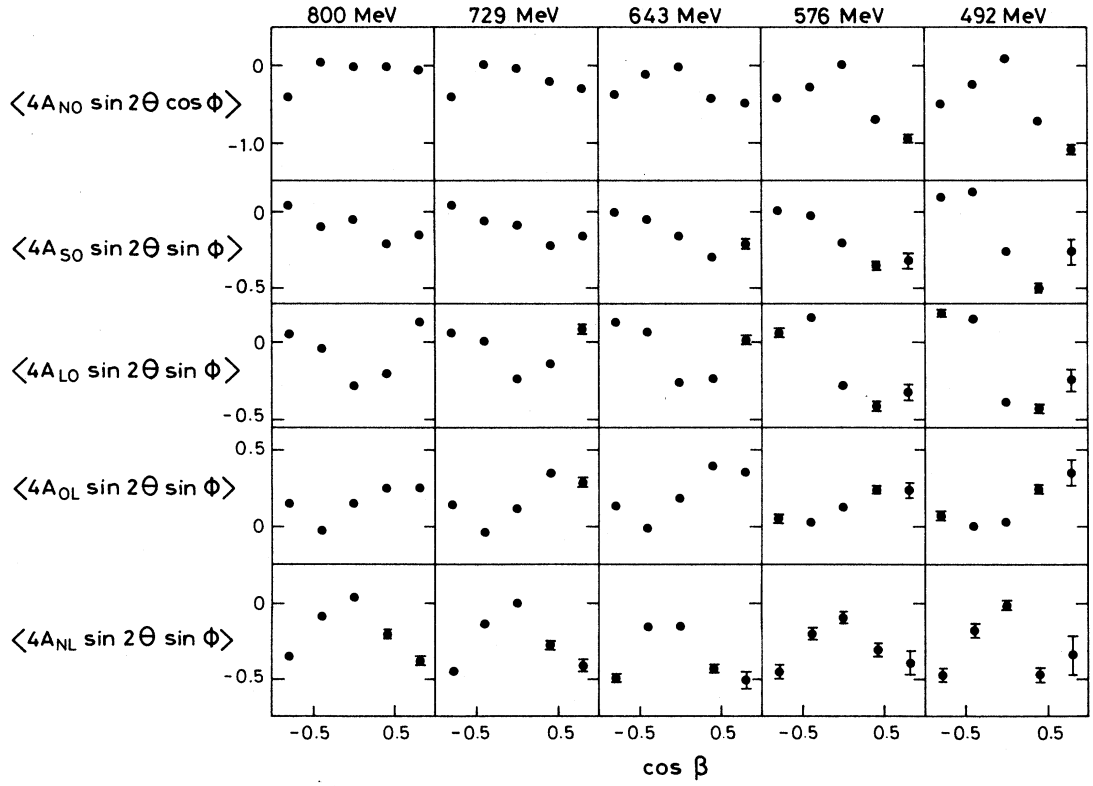

FIG. 14. Averages over our acceptance $\langle 4A_{NO}\sin 2\theta\cos\Phi\rangle$ and $\langle 4A_{SO}\sin 2\theta\sin\Phi\rangle$, $\langle 4A_{LO}\sin 2\theta\sin\Phi\rangle$, $\langle 4A_{OL}\sin 2\theta\sin\Phi\rangle$, $\langle 4A_{NL}\sin\theta\sin\Phi\rangle$, plotted against $\cos\beta$.

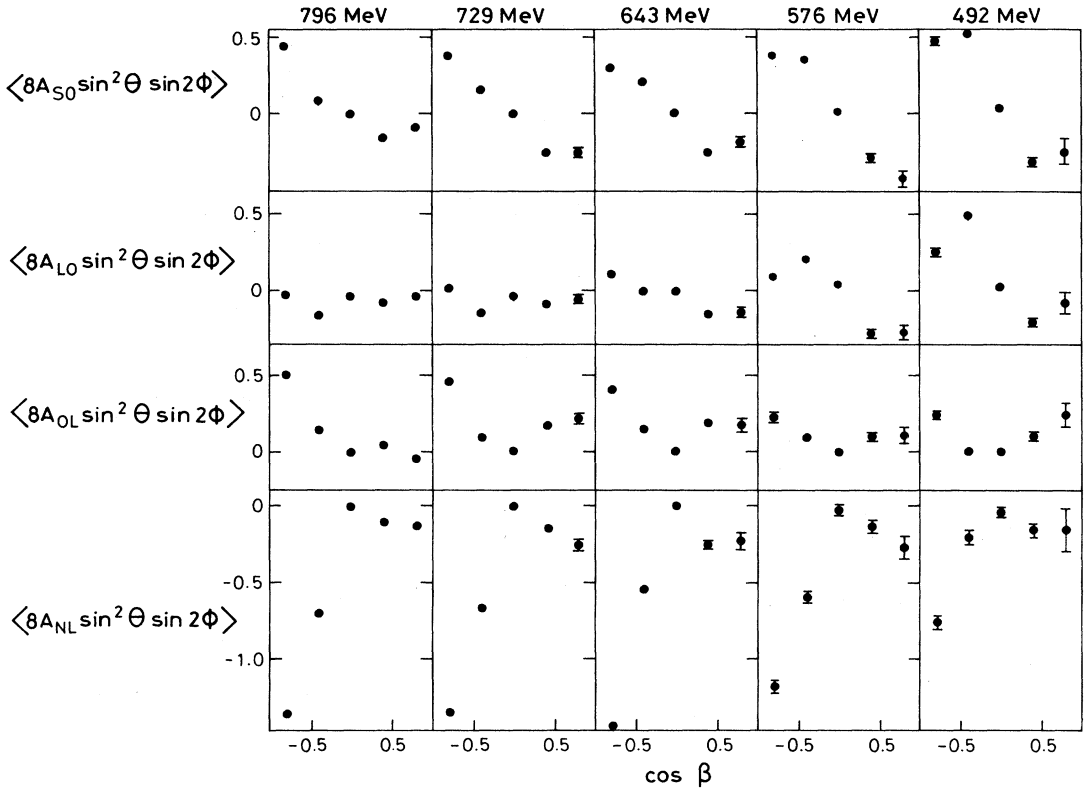

FIG. 15. Averages over our acceptance $\langle 8A_{SO}y\rangle$, $\langle 8A_{LO}y\rangle$, $\langle 8A_{OL}y\rangle$, and $\langle 8A_{NO}y\rangle$ where $y=\sin^2\theta\sin 2\Phi$.

sults with theirs is indirect confirmation of our normalization. The data of Wicklund *et al.* have somewhat larger ($\pm 10\%$) normalization uncertainty.

Results have also been compared with those of Waltham *et al.*[4] For A_{NO} and A_{LL} the two experiments agree within two standard deviations for the events within the acceptance of our experiment. For A_{SL}, the TRIUMF results were interpreted as indicating $A_{SL}\simeq 0$, though slight positive values were possible. The much higher statistics of the present experiment show that A_{SL} at 492 MeV is, in fact, definitely positive; any disagreement between the two experiments is statistically marginal.

A. The *np* final-state interaction

In the TRIUMF data, a strong *np* final-state interaction (FSI) peak was observed at low M_{NN}. In it, A_{NO} and A_{ON} dropped sharply while A_{NN} remained steady. This was interpreted as indicating that the *np* FSI enhanced the $^1D_2\rightarrow{}^5S_2$ amplitude with respect to other partial waves. This amplitude in the $N\Delta$ basis projects on to the $(NN)\pi$ basis in two states: $^3S_1$ with a *P*-wave π and $^3P_2$ with an *S*-wave π. The idea was that the *P*-wave π can resonate simultaneously with both nucleons, which in turn interact attractively through the $^3S_1$ interaction. However, we now demonstrate that the actual situation is more complicated.

TABLE I. A comparison of results with those of Wicklund *et al.*

Energies (MeV) This experiment	Wicklund *et al.* (Ref. 33)	χ^2	Number of bins
576	569	A_{NO} 105.0	91
		A_{SO} 77.4	91
		A_{LO} 84.2	91
796	806	A_{NO} 200.7	192
		A_{SO} 121.9	192
		A_{LO} 191.0	192

In the amplitude analysis, we have tried including a Watson-Migdal FSI enhancement factor. If it is applied to all partial waves, it has no effect on spin-dependent observables, but simply enhances the cross section. It is interesting, however, to try its effect on the $^1D_2$ amplitude alone. We have used a Jost junction which fits the *np* $^3S_1$ phase shift accurately from threshold to 400 MeV. It has two effects: (a) it enhances the strength of the amplitude by up to a factor of 4 and (b) it rotates the phase by δ_{NN}. The latter has a very large effect over a range of *NN* masses extending well above threshold. Remember that the *NN* $^3S_1$ phase shift drops from 180° at threshold to 90° at a laboratory energy of 18 MeV and 45° only at 94 MeV. We find that introducing this FSI into the $^1D_2$ amplitude alone worsens χ^2 by ~ 180 at 492 MeV and by similar amounts at higher energies; the resulting fit is shown by the dashed line in Fig. 16. It is in clear disagreement with A_{NO} and A_{SL} data.

The conclusion is that the data are best fitted without any significant phase rotation implied by the Jost func-

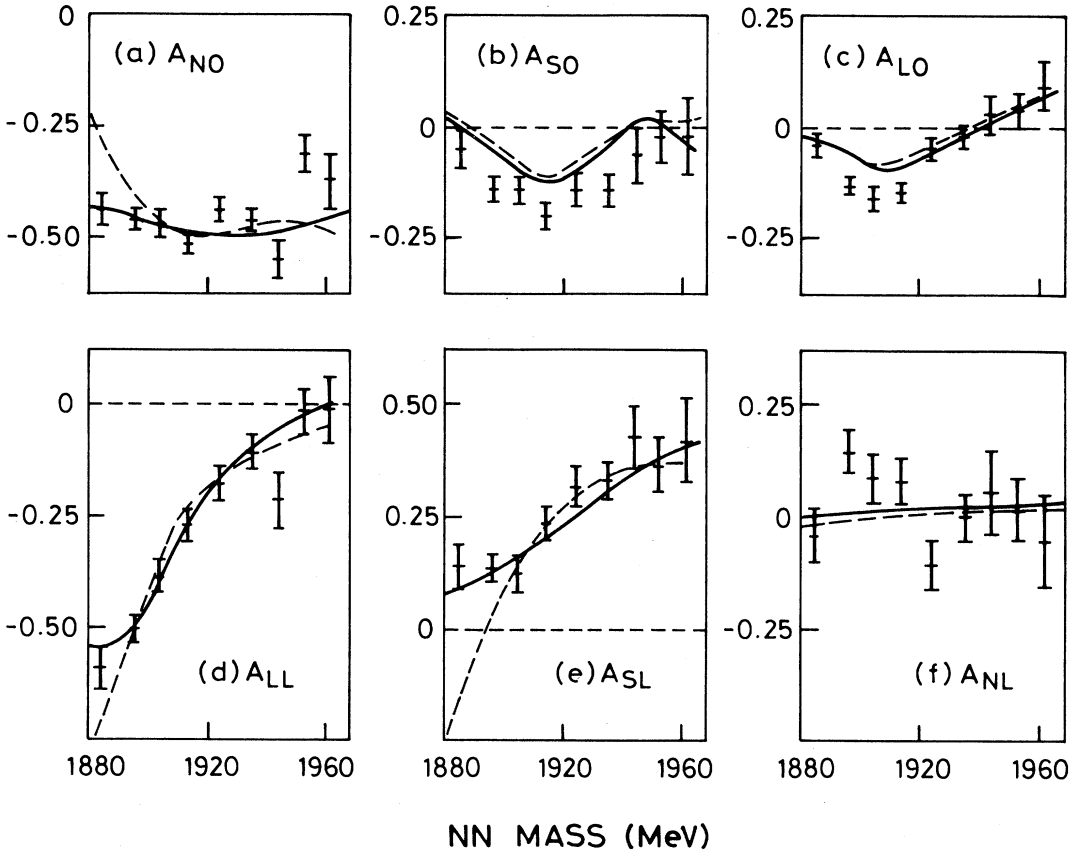

FIG. 16. One-dimensional projections of (a) A_{NO}, (b) A_{SO}, (c) A_{LO}, (d) A_{LL}, (e) A_{SL}, and (f) A_{NL} against NN mass at 492 MeV. Full curves are from the isobar fit; dashed curves include the NN FSI in $^1D_2 \to {}^5S_2$ only.

tion, or, alternatively, by the same phase rotation in all partial waves. It implies that an alternative explanation is required for the TRIUMF observation that A_{ON} and A_{NO} drop from values of about -0.4 outside the FSI peak to values of about -0.1 in it. We now present such an alternative explanation.

Low NN mass implies a πN mass close to the maximum kinematically allowed. Table II shows that A_{NO} begins to drop at the highest M values. There are several conspiring effects producing this result. At intermediate values of M, the $NN(^1D_2) \to N\Delta(^5S_2)$ and $NN(^3P_1) \to NS(^3S_1)$ amplitudes dominate, and their interference generates the large A_{NO}. At 492 MeV, $\delta_{NN}(^3P_1) \simeq -40°$, $\delta_{NN}(^1D_2) \simeq 13°$, and $\delta_{N\Delta}(^5S_2) = 44.4°$.

TABLE II. Comparison of one-dimensional projections of A_{NO} against M from the present experiment at 492 MeV and the TRIUMF experiment, Ref. 4 at 510 MeV.

M (MeV)	A_{NO} This experiment	M (MeV)	A_{NO} Ref. 4
1094	-0.275 ± 0.081	1090	-0.086 ± 0.244
1112	-0.297 ± 0.029	1110	-0.457 ± 0.110
1130	-0.420 ± 0.020	1130	-0.606 ± 0.078
1151	-0.498 ± 0.016	1150	-0.465 ± 0.043
1161	-0.431 ± 0.027	1169	-0.291 ± 0.029

At the highest M value, the phase of the S amplitude arising from πN S waves is $\simeq -20°$ and rising slowly with M, while the phase of the Δ amplitude is 28° and rising rapidly with M. Thus the two interfering amplitudes differ in phase by 145.4° at the highest M, and A_{NO} is dropping rapidly as this phase difference increases with M. In addition, the $NN(^1D_2) \to N\Delta(^5S_2)$ amplitude makes much the larger contribution to $d\sigma/d\Omega$, and its rapid increase with M is depressing A_{NO}. Finally, the other amplitudes with $L_{N\Delta} = 1$ are rising rapidly with k (Δ c.m. momentum) in the FSI peak, and contribute to A_{NO} with the opposite sign. From the present experiment, these other small amplitudes are hard to assess accurately. However, it is plausible that in the FSI peak the amplitudes will be close to those for $pp \to d\pi$ [the alternative possibility of np $^1S_0$ with a $1=0$ pion projects on to the $NN(^3P_0) \to NS(^1S_0)$ amplitude, which we find to be negligible, while np $^1S_0$ with a $1=1$ pion is forbidden by the Pauli principle]. Thus one expects A_{NO} in the FSI peak to assume a value close to that for $pp \to d\pi$. The geometry of the TRIUMF experiment was such that the FSI peak was detected with pions scattered to the right in the c.m. angular range of 13° to 50°. In this geometry, the mean value of A_{NO} for $pp \to d\pi^+$ is -0.02 at 420 MeV, -0.13 at 465 MeV, and -0.25 at 510 MeV. These values are compatible with the TRIUMF observations in the FSI peak. Our conclusions are that (a) the explana-

tion given in Ref. 4 for the drop in A_{NO} in the FSI peak was an oversimplification, and (b) there is no disagreement between TRIUMF data and those of the present experiment, which do not go to small enough neutron laboratory angles to reach the $d\pi^+$ kinematics.

In view of the huge complexity of projecting the NN FSI into the $N\Delta$ and NS basis (prohibitive in computer time), the amplitude analysis simply omits points with $M_{NN} < 1890$ MeV. Inspection of $d\sigma/d\Omega$ data of Hancock *et al.* shows that this excludes the region of dominant FSI effects.

V. CONCLUSIONS AND DISCUSSION

Six phase-sensitive observables and A_{LL} have been measured at five energies from 492 to 796 MeV. There is rather little variation with energy in most of the data. What there is, notably in A_{NO}, is explained by the phase $\delta_{N\Delta}$ for $^1D_2 \rightarrow {}^5S_2$, which falls from 44° at 492 MeV to 11° at 796 MeV. Final-state np interactions have no visible effect on spin-dependent observables (Fig. 16).

Phases of $^1D_2 \rightarrow {}^5S_2$ and $^3P_2$ $NN \rightarrow N\Delta$ amplitudes are well determined everywhere, and $^3F_3 \rightarrow {}^5P_3$ at 643 MeV and above. Phases of $^1S_0 \rightarrow {}^5D_0$, $^3P_0 \rightarrow {}^3P_0$, and $^3P_1$ amplitudes are determined at the higher energies, and the fits at lower energies are consistent with a smooth extrapolation to threshold. Results are displayed in Figs. 8 and 9.

Other than in $\delta_{N\Delta}(^5S_2)$, there is no evidence for dramatic phase variations, nor for unexpected magnitude variations. The appearance of the amplitudes is qualitatively what one expects for an inelastic threshold, and there is no evidence for resonant behavior.

The phase $\delta_{N\Delta}(^5S_2)$, shown in Fig. 8, is interesting. A similar result has been obtained by Ferreira *et al.*[38] from an analysis of πd elastic scattering data. It is a question for theorists as to how to explain this phase variation quantitatively. When we undertook this experiment, we envisaged that a conventional dibaryon resonance would manifest itself by a large loop in the Argand diagram in the $N\Delta$ channel to which it reputedly has the strongest branching ratio. Our results are incompatible with such a resonance.

The phase variation in $N\Delta(^5S_2)$, however, clearly requires some nearby discontinuity. Does it necessitate a nearby pole, as Hoshizaki[39] argues, or does the phase variation follow from analyticity and the opening of the $N\Delta$ threshold? The $N\Delta \rightarrow N\Delta$ cross section will have a roughly $1/v$ dependence near threshold because of the coupling to the open NN channel. The imaginary part of the amplitude will have a step at threshold to a roughly constant value dependent on the $N\Delta$ scattering length. This step in the imaginary part will inevitably lead, via analyticity, to rapid energy dependence in the real part, hence phase variation. A full analysis demands, at least, an inclusion of the known π exchange pole and treatment of the coupled NN channel, where the phase of the $^1D_2$ amplitude is known. The quantitative question still at issue is whether, as in the NN system, an additional bound or virtual state is required or whether the threshold alone accounts for the data.

Whichever is the case, there is certainly a large positive $N\Delta$ phase near threshold. It is interesting to explore its consequences for both nuclear matter and nuclear physics. It will soften the equation of state for nuclear matter at high densities. We also remark that experiments such as that of Contardo *et al.*[40] have consistently observed the Δ lower in mass in N nuclear reactions than in free N scattering; this could be a consequence of a Δ being attracted by all the nucleons of a nucleus.

ACKNOWLEDGMENTS

We gratefully acknowledge the enthusiastic support of the LAMPF accelerator crew and also the polarized target group, led by Dr. J. Jarmer. We are grateful to Dr. A. S. Clough, Dr. N. M. Stewart, Mr. R. Lamb, Dr. O. B. van Dyck, Dr. J. A. McGill, Mr. M. Bachmann, and Mr. S. Cummings for assistance during the runs. We thank Dr. J. E. Simmons for the loan of the polarized target cryostat and electronics, and Dr. L. C. Northcliffe and Dr. G. Glass for the loan of two MWPC's. The experiment was supported by the U.S. Department of Energy and by the Science and Engineering Research Council (SERC). We also gratefully acknowledge comments on the interpretation of the results from Professor J. Speth and Professor E. Lomon.

*Present address: SLAC, P.O. Box 4349, Stanford, CA 94305.
†Present address: Los Alamos National Laboratory, Los Alamos, NM 87545.

[1]M. Roos *et al.*, Phys. Lett. **111B**, 1 (1982).
[2]M. P. Locher, M. E. Sainio, and A. Svarc, Adv. Nucl. Phys. **17**, 47 (1986).
[3]R. L. Shypit *et al.*, Phys. Rev. Lett. **60**, 901 (1988).
[4]C. E. Waltham *et al.*, Nucl. Phys. **A433**, 649 (1985).
[5]I. P. Auer, E. Colton, D. Hill, K. Nield, B. Sandler, H. Spinka, Y. Watanabe, A. Yokosawa, and A. Beretvas, Phys. Lett. **67B**, 113 (1977); I. P. Auer, A. Beretvas, E. Colton, D. Hill, K. Nield, H. Spinka, D. Underwood, Y. Watanabe, and A. Yokosawa, *ibid.* **70B**, 475 (1977); I. P. Auer, E. Colton, H. Halpern, D. Hill, H. Spinka, G. Theodosiou, D. Underwood, Y. Watanabe, and A. Yokosawa, Phys. Rev. Lett. **41**, 354 (1978).
[6]H. Hidaka, A. Beretvas, K. Nield, H. Spinka, D. Underwood, Y. Watanabe, and A. Yokosawa, Phys. Lett. **70B**, 479 (1977).
[7]N. Hoshizaki, Prog. Theor. Phys. **57**, 1079 (1977); **58**, 716 (1977); **60**, 1796 (1978); **61**, 129 (1979).
[8]R. A. Arndt, Phys. Rev. **165**, 1834 (1968).
[9]W. M. Kloet and R. R. Silbar, Phys. Rev. Lett. **45**, 970 (1980).
[10]W. M. Kloet, J. A. Tjon, and R. R. Silbar, Phys. Lett. **99B**, 80 (1981).
[11]J. Niskanen, Phys. Lett. **112B**, 1 (1982).
[12]B. J. VerWest, Phys. Rev. C **25**, 482 (1982).
[13]S. Furuichi, K. Nakamura, and H. Suzuki, in Proceedings of the Meeting on Exotic Resonances, Hiroshima, 1978 (Univer-

sity of Hiroshima Report No. HUPD-7813, 1978).
[14]B. J. Edwards, Phys. Rev. D **23**, 1978 (1981).
[15]R. Bhandari, R. A. Arndt, L. D. Roper, and B. J. VerWest, Phys. Rev. Lett. **46**, 1111 (1981).
[16]R. A. Arndt, J. S. Hyslop III, and L. D. Roper, Phys. Rev. D **35**, 128 (1987).
[17]W. M. Kloet and J. A. Tjon, Phys. Lett. **106B**, 24 (1981).
[18]D. V. Bugg, Nucl. Phys. **A437**, 534 (1985).
[19]N. Hiroshige, W. Watari, and M. Yonezawa, Prog. Theor. Phys. **72**, 1146 (1984).
[20]A. V. Kravtsov, M. G. Ryskin, and I. I. Strakovsky, J. Phys. G **9**, L187 (1983).
[21]N. Hiroshige, M. Kawasaki, K. Takabayashi, W. Watari, and M. Yonezawa, Prog. Theor. Phys. **72**, 1287 (1984); **74**, 193 (1985).
[22]N. Hiroshige, M. Kawasaki, W. Watari, and M. Yonezawa, Prog. Theor. Phys. **74**, 1161 (1985).
[23]F. H. Cverna, P. R. Bevington, M. W. McNaughton, H. B. Willard, N. S. P. King, and D. R. Giebink, Phys. Rev. C **23**, 1698 (1981).
[24]A. D. Hancock *et al.*, Phys. Rev. C **27**, 2742 (1983).
[25]T. S. Bhatia *et al.*, Phys. Rev. C **28**, 2071 (1983).
[26]G. Glass *et al.*, Phys. Lett. **129**, 27 (1983).
[27]C. Hollas *et al.*, Phys. Rev. Lett. **55**, 29 (1985).
[28]P. C. Gugelot, S. Kullander, G. Landau, F. Lemeilleur, and J. Yonnet, Nucl. Phys. **B37**, 93 (1972).
[29]J. A. McGill, C. Glasshauser, K. Jones, S. K. Nanda, M. Barlett, R. Fergerson, J. A. Marshiel, E. C. Milner, and G. W. Hoffmann, Phys. Lett. **134B**, 157 (1984).
[30]P. J. Riley *et al.*, Phys. Lett. B **197**, 23 (1987).
[31]J. Hudomalj-Gabitzch *et al.*, Phys. Rev. C **18**, 2666 (1978).
[32]B. E. Bonner, C. L. Hollas, C. R. Newson, P. J. Riley, G. Glass, M. Jain, and B. J. VerWest, Phys. Rev. D **27**, 497 (1983).
[33]A. B. Wicklund *et al.*, Phys. Rev. D **35**, 2670 (1987).
[34]G. G. Ohlsen, J. L. McKibben, G. P. Lawrence, P. W. Keaton, Jr., and D. D. Armstrong, Phys. Rev. Lett. **27**, 599 (1971); M. W. McNaughton, P. R. Bevington, H. B. Willard, E. Winkelmann, E. P. Chamberlin, F. H. Cverna, N. S. P. King, and H. Willmes, Phys. Rev. C **23**, 1128 (1981); M. W. McNaughton and E. P. Chamberlin, *ibid.* **24**, 1778 (1981).
[35]M. Jacob and G. C. Wick, Ann. Phys. (N.Y.) **7**, 404 (1959).
[36]M. G. Ryskin and I. I. Strakovsky, Phys. Rev. Lett. **61**, 2384 (1988).
[37]R. L. Shypit *et al.*, Phys. Rev. Lett. **61**, 2385 (1988).
[38]E. Ferreira, S. C. B. de Andrade, and H. G. Dosch, Phys. Rev. C **36**, 1916 (1987).
[39]N. Hoshizaki, University of Kyoto report, 1988 (unpublished).
[40]D. Contardo *et al.*, Phys. Lett. **168B**, 331 (1986).